ELSEVIER

Computer Methods and Programs in Biomedicine 54 (1997) 141–150

Computer Methods and Programs in Biomedicine

CONV—convolution for responses to a finite diameter photon beam incident on multi-layered tissues

Lihong Wang [a,*], Steven L. Jacques [b], Liqiong Zheng [c]

[a] *Bioengineering Program, Texas A&M University, College Station, TX 77843-3120, USA*
[b] *Oregon Medical Laser Center, St. Vincent Hospital, 9205 S.W. Barnes Road, Portland, OR 97225, USA*
[c] *Computer Information Services, Texas A&M University, College Station, TX 77843-3142, USA*

Received 7 August 1996; received in revised form 27 February 1997; accepted 21 April 1997

Abstract

A convolution program (CONV) solving responses to a collimated finite diameter photon beam perpendicularly incident on a multi-layered tissue has been coded in ANSI Standard C, hence, the program can be executed on various computers. The program, employing an extended trapezoidal rule for integration, convolves the responses to an infinitely narrow photon beam computed by a companion program (MCML). Dynamic data allocation is used for CONV as well as MCML, therefore, the number of tissue layers and grid elements of the grid system can be varied at run time. The potential error due to not scoring the first photon–tissue interactions separately is illustrated. The program, including the source code, has been in the public domain since 1992 and can be downloaded from the web site at http://biomed.tamu.edu/~lw. © 1997 Elsevier Science Ireland Ltd.

Keywords: Convolution; Photon transport; Tissue optics; Standard C; Dynamic allocation

1. Introduction

Monte carlo modeling has been used frequently to simulate photon propagation in tissues [1–8] which provides good accuracy and flexibility compared with other theories. However, a long computational time used to trace a large number of photons is usually required to achieve sufficiently precise results.

We have written a companion program named MCML, in Standard C for Monte Carlo simulations of photon propagation in multi-layered tissues [9,10], which deals only with responses to an infinitely narrow photon beam normally incident on the surface of a multi-layered tissue (impulse responses). However, all photon beams have finite size in reality. We could use the Monte Carlo simulation to compute the response to a finite size photon beam directly by distributing the initial positions of launched photons. The only problem

* Corresponding author. Tel. +1 409 8479040; fax: +1 409 8479005; e-mail: LWang@tamu.edu.

PII S0169-2607(97)00021-7

with this approach is that it requires tracing an even larger number of photon packets to reach an acceptable variance than simulating the responses of an infinitely narrow photon beam. Therefore, this method is not computationally efficient, although sometimes it may be the only approach for tissue configurations without proper symmetry, such as a tissue with an irregularly buried object. Fortunately the responses to a finite size photon beam incident onto the multi-layered tissues can be obtained through convolution over the responses to an infinitely narrow beam.

In the following sections, we will describe the mathematics and numerical computation of the convolution (Section 2), present some sample computational results (Section 3) and summarize (Section 4).

2. Convolution

This section will discuss the principle and numerical computation of convolving Monte Carlo simulation results of an infinitely narrow photon beam to yield the responses to photon beams of finite size where the photon beams are always perpendicular to the surface of a multi-layered tissue. The convolution process is implemented in a program called CONV. Like MCML, it is written in ANSI Standard C, hence, it can be executed on various computers, provided they have Standard C compilers. Only Gaussian beams and circular flat beams are considered in the program. To check the program, we compared our convolution results with those of other investigators [11].

2.1. Principles of convolution

The system, which is a multi-layered tissue with a collimated photon beam perpendicularly incident on the tissue surface, is linear and invariant. The linearity means that if the input intensity of the infinitely narrow photon beam is multiplied by a factor, the responses will be multiplied by the same factor. It also means that the response to two photon beams is the sum of the responses to each photon beam. The invariance means that when the photon beam is shifted horizontally by a distance in a certain direction, the responses will also be shifted by the same distance horizontally and in the same direction. Therefore, according to the profile of the finite size photon beam, its response can be convolved over the Green's function that is the response of an infinitely narrow photon beam.

Impulse responses are simulated with MCML first, where a cartesian coordinate system is set up on the tissue [9]. The origin of the coordinate system is the photon incident point on the tissue surface; the z-axis is always the normal of the surface pointing toward the inside of the tissue; therefore, the xy-plane is on the tissue surface.

The responses simulated in the Monte Carlo modeling can be internal absorption, reflectance, or transmittance. We denote the responses to a photon beam of finite size generally as $C(x, y, z)$, and denote the Green's function corresponding to the type of response under consideration as $G(x, y, z)$. Because the photon beam is perpendicularly incident on the tissue surface and the multi-layered tissue has cylindrical symmetry, the function $G(x, y, z)$ possesses cylindrical symmetry. If the collimated photon beam as the source has the intensity profile $S(x, y)$ the responses can be obtained through convolution [2]:

$$C(x, y, z) = \int_{-\infty}^{\infty}\int_{-\infty}^{\infty} G(x-x', y-y', z)S(x', y')\,dx'\,dy', \tag{1}$$

which is reformulated with $x'' = x - x'$ and $y'' = y - y'$:

$$C(x, y, z) = \int_{-\infty}^{\infty}\int_{-\infty}^{\infty} G(x'', y'', z)S(x-x'', y-y'')\times dx''\,dy'', \tag{2}$$

In Eq. (1), the Green's function is a function of the distance between the source point (x', y') and the observation point (x, y), where the distance is:

$$d' = \sqrt{(x-x')^2 + (y-y')^2}. \tag{3}$$

If the intensity profile $S(x', y')$ of the source also has cylindrical symmetry, $S(x', y')$ is only a function of the radius, which is the distance between the source point (x', y') and the origin of the coordinate system, i.e.:

$$r' = \sqrt{x'^2 + y'^2}. \tag{4}$$

Therefore, Eqs. (1) and (2) can be reformulated considering these symmetries:

$$C(x, y, z) = \int_{-\infty}^{\infty}\int_{-\infty}^{\infty} G(\sqrt{(x-x')^2 + (y-y')^2}, z) \times S(\sqrt{x'^2 + y'^2})\, dx'\, dy' \tag{5}$$

$$C(x, y, z) = \int_{-\infty}^{\infty}\int_{-\infty}^{\infty} G(\sqrt{(x''^2 + y''^2}, z) \times S(\sqrt{(x-x'')^2 + (y-y'')^2})\, dx''\, dy''. \tag{6}$$

Because the response $C(x, y, z)$ will have the same cylindrical symmetry, the problem can be more easily handled in a cylindrical coordinate system, where Eqs. (5) and (6) can be rewritten:

$$C(r, z) = \int_0^{\infty} S(r') r'\left[\int_0^{2\pi} G(\sqrt{r^2 + r'^2 - 2rr'\cos\theta'}, z)\, d\theta'\right] \times dr', \tag{7}$$

$$C(r, z) = \int_0^{\infty} G(r'', z) r''\left[\int_0^{2\pi} S(\sqrt{r^2 + r''^2 - 2rr''\cos\theta''})\, d\theta''\right] \times dr''. \tag{8}$$

The variable transformation is illustrated in more detail in [7]. Eq. (8) is more advantageous than Eq. (7) for computation because the integration over θ'' is independent of z; hence, for all depths z this integration need only be computed once. As presented subsequently, in some cases the integral over θ'' can be solved in terms of Bessel functions or analytically, therefore, the 2-dimensional integral is converted into a 1-dimensional integral, which can be computed significantly faster than a 2-dimensional integral. We will consider a Gaussian beam and a circular flat beam as examples of cylindrical symmetry where Eq. (8) can be further simplified.

2.2. Convolution over Gaussian beams

In the case of a Gaussian beam, if the divergence is ignored, the above convolution can be applied. The $1/e^2$ radius of the Gaussian beam is denoted by R, and the beam intensity profile is:

$$S(r') = S_0 \exp(-2(r'/R)^2), \tag{9}$$

where the intensity in the center $(r = 0)$, S_0, is related to the total power P by:

$$S_0 = 2P/(\pi R^2). \tag{10}$$

Substituting Eq. (9) into Eq. (8), the convolution becomes:

$$C(r, z) = S(r)\int_0^{\infty} G(r'', z)\exp(-2(r''/R)^2)\left[\int_0^{2\pi}\exp(4rr''\cos\theta''/R^2)\, d\theta''\right] r''\, dr'', \tag{11}$$

where the integration in the square brackets resembles the integral representation of the modified Bessel function [12]:

$$I_0(x) = \frac{1}{2\pi}\int_0^{2\pi}\exp(x\sin\theta)\, d\theta, \tag{12}$$

where I_0 is the zero order modified Bessel function, which can be reformulated converting the sine function into a cosine function:

$$I_0(x) = \frac{1}{2\pi}\int_0^{2\pi}\exp(x\cos\theta)\, d\theta. \tag{13}$$

Eq. (11) can be rewritten by using Eq. (13):

$$C(r, z) = S(r)\int_0^{\infty} G(r'', z)\exp(-2(r''/R)^2) \times I_0(4rr''/R^2)2\pi r''\, dr''. \tag{14}$$

2.3. Convolution over circular flat beams

For a circular flat beam, which is collimated and homogeneous within a radius R, the source function becomes:

$$S(r') = \begin{cases} P/(\pi R^2) & \text{if } r' \le R \\ 0 & \text{if } r' > R \end{cases} \quad (15)$$

where P is the total power of the beam. Substituting Eq. (15) into Eq. (8), the convolution becomes:

$$C(r, z) = P/(\pi R^2) \int_0^{\infty} G(r'', z) I_\theta(r, r'') 2\pi r'' \, dr'', \quad (16)$$

where the function $I_\theta(r, r'')$ is:

$$I_\theta(r, r'') = \begin{cases} 1 & \text{if } R \ge r + r'' \\ \frac{1}{\pi} \cos^{-1}((r^2 + r''^2 - R^2)/(2rr'')) & \text{if } |r - r''| \le R < r + r'' \\ 0 & \text{if } R < |r - r''| \end{cases} \quad (17)$$

From Eq. (17) the integral limits in Eq. (16) can be changed to a finite region:

$$C(r, z) = P/(\pi R^2) \int_a^{r+R} G(r'', z) I_\theta(r, r'') 2\pi r'' \, dr'', \quad (18)$$

where

$$a = \text{Max}(0, r - R), \quad (19)$$

where the function Max takes the greater of the two arguments.

As a special case of a circular flat beam, we let the radius R approach infinity, which represents an infinitely wide flat beam. In this case, the total power P also approaches infinity, but we can use the power density to describe the intensity of the beam. The convolution for this beam can be accomplished by simply letting $R \to \infty$ and $P/(\pi R^2) \to S$, where S is the power density or irradiance (W/cm^2) in Eq. (18). This substitution leads $I^\theta(r, r'')$ to a constant 1, and Eq. (18) becomes:

$$C(r, z) = S \int_0^{\infty} G(r'', z) 2\pi r'' \, dr''. \quad (20)$$

This equation implies that in a Monte Carlo simulation using MCML, if the photon weight over all the r grid elements for a given z grid is totaled, and then the sum is divided by the total number of traced photons, the result will be the absorption density as a function of z for an infinitely wide beam with a unity power density.

2.4. Numerical solution to the convolution

During Monte Carlo simulations, a grid system is set up [9]. A 2-dimensional homogeneous grid system is set up in the r and z directions. The grid separations are Δr and Δz in the r and z directions, respectively. The total numbers of grid elements in the r and z directions are N_r and N_z, respectively.

When photon beams are Gaussian or circular flat beams the 2-dimensional integrations are converted into 1-dimensional integrations. Because the Monte Carlo simulation scores physical quantities to discrete grid points, the best choice of an integration algorithm is the extended trapezoidal rule, which has been written in C called qtrap( ) by Press et al. [13]. The function qtrap( ) is a driver routine for another function trapzd( ) which actually implements the extended trapezoidal rule integration. Press et al. state "increased sophistication will usually translate into a higher order method whose efficiency will be greater only for sufficiently smooth integrands. qtrap Is the method of choice, e.g. for an integrand which is a function of a variable that is linearly interpolated between measured data points".

Another choice of integration is evaluating the integrand at the original grid points. However, this approach does not have any control over the integration accuracy. For a given accuracy sometimes this approach is more accurate than required, which is a waste of computational time, and sometimes is less accurate, which does not meet expectations. For example, the number of original grid elements in the r direction is 50, and we want to convolve the responses over a circular flat beam with a radius of R which is about $5\Delta r$.

To compute $C(0, z)$ for a circular flat beam using Eq. (18), the integral range, from 0 and R, only covers $5\Delta r$. This means only five function evaluations will be completed, which may yield an unacceptable answer. In contrast, the extended trapezoidal rule performs the correct number of function evaluations until the computation reaches the user-specified level of accuracy.

We have slightly modified the original function qtrap( ) so that it takes the required degree of accuracy as an argument to the function. Therefore, the users of the program CONV can change the allowed error at run time.

The sequence of integrand evaluations [13] used in the extended trapezoidal rule is shown in Fig. 1a. "Sequential calls to the routine trapzd( ) incorporate the information from previous calls and evaluate the integrand only at those new points necessary to refine the grid. The bottom line shows the total of function evaluations after the fourth call" [13]. If we are integrating f(x) over $[a, b]$, we evaluate f(a) and f(b) in the first step as noted by 1 and 2 in Fig. 1a. This step will not be sufficiently accurate unless the function is linear. To refine the grid, we evaluate f($(a+b)/2$) in the second step as noted by 3, and we continue this process until the integration evaluation reaches the specified accuracy.

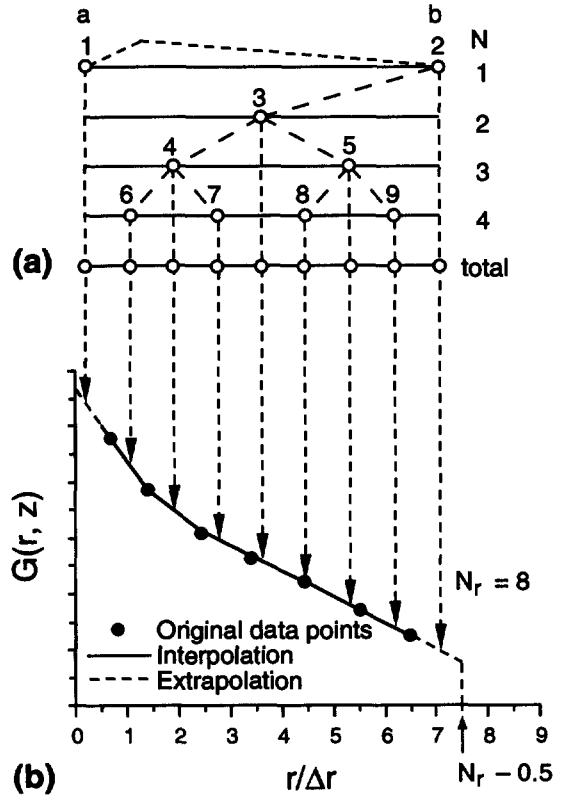

Fig. 1. (a) Integrand evaluation sequence in extended trapezoidal rule of integration. (b) Interpolation and extrapolation of the physical quantities. In this example, the number of grid elements in the r direction N_r is set to 8. The symbols a and b are the integral limits. The arrows point to the places where the integrand is evaluated.

2.5. Interpolation and extrapolation of physical quantities

The physical quantities under discussion have been computed using MCML over a grid system. As discussed in [9] the optimized r coordinate, instead of the center, for the scored physical quantities for an r grid element is:

$$r_b = \left[(i+0.5) + \frac{1}{12(i+0.5)}\right]\Delta r, \tag{21}$$

where i is the index to the grid element ($0 \le i \le N_r - 1$). For the first grid element, the optimized r coordinate is $(2/3)\Delta r$ instead of $(1/2)\Delta r$. The offset between the optimized and the centered coordinates in each grid element decreases as the index i increases. The convolution error of using the centers will be illustrated in the next section.

In Fig. 1, the function qtrap( ) will need to evaluate the integrand (hence the physical quantities) at points that may not be the original grid points. Linear interpolations are used for those points that fall between two original grid points, and linear extrapolations are used for those points that fall beyond the original grid system (Fig. 1). The circles represent the original scored values at the grid points, and the solid lines and the dashed lines represent the interpolation and extrapolation, respectively. For a given number of grid elements in the r direction ($N_r = 8$ in this picture), the extrapolation is computed only up to $(N_r - 0.5)\Delta r$ because the linear extrapolation can be unreliable if extended too far, hence, the physical quantity beyond $(N_r - 0.5)\Delta r$ is set to zero.

In the computation by MCML [9], the last cells in the r direction are used to collect the photons that do not fit into the grid system and do not represent the local physical quantities. Therefore, the upper limit of extrapolation is $(N_r - 0.5)\Delta$ir instead of $(N_r - 0.5)\Delta r$. In a word, the physical quantities are non-zero in the interval $[0, r_{max}]$, where r_{max} is:

$$r_{max} = (N_r - 0.5)\Delta r. \tag{22}$$

2.6. Integrand evaluation for Gaussian beams

In Eq. (14), the evaluation of the physical quantities is only part of the integrand evaluation for convolution over a Gaussian beam. Although the integration must converge for physical reasons the form of Eq. (14) may not be directly computable digitally because the modified Bessel function increases rapidly as the argument increases and may exceed the limit which the computer can hold (10^{+38} for some computers), which is called overflow. Therefore, to compute Eq. (14), a proper reformulation is required. We note that the modified Bessel function in the region where the argument is large has the following approximation:

$$I_0(x) \approx \exp(x)/\sqrt{2\pi x} \quad \text{for large } x, \tag{23}$$

Therefore, if we extract the exponential term from $I_0(\,)$ we ensure that the modified Bessel function decreases as the argument increases. We define the following new function based on $I_0(\,)$:

$$I_{0e}(x) = I_0(x)\exp(-x), \tag{24}$$

or

$$I_0(x) = I_{0e}(x)\exp(x), \tag{25}$$

$I_{0e}(\,)$ is always bounded. Eq. (23) demonstrates the asymptotic behavior of the function $I_0(\,)$, hence, Eq. (24) does not carry any approximations. Substituting Eqs. (9), (10) and (25) into Eq. (14), it becomes:

$$C(r,z) = \frac{4P}{R^2}\int_0^{\infty} G(r'',z)\exp\left[-2\left(\frac{r''-r}{R}\right)^2\right] \times I_{0e}\left(\frac{4rr''}{R^2}\right)r''\,dr''. \tag{26}$$

Because both the exponential term and the $I_{0e}(\,)$ term decrease, the integrand can be computed without causing overflow.

The computation speed is another issue. We found that the evaluation of the $\exp(\,)I_{0e}(\,)$ in Eq. (26) is a major part of the computation for each integration, which can take up to 90% of the computational time depending upon the specific problem. For multi-variant physical quantities (e.g. the internal fluence as a function of r and z), the convolution may repeatedly evaluate the $\exp(\,)I_{0e}(\,)$ in Eq. (26) at the same r coordinate as the integration is computed for different z coordinates.

Therefore, if we can save the function evaluations, i.e. the computations of $\exp(\,)I_{0e}(\,)$ in Eq. (26), during the convolution for one z coordinate, then we can save a lot of computational time. However, the integration is computed iteratively until a given precision is reached. Hence, the number of function evaluations is unknown in advance, and we can save only the function evaluations with dynamic data allocation. Because the evaluation sequence of the trapezoidal integration qtrap( ) resembles a binary tree as shown in Fig. 1a we used a binary tree to store the function evaluations which is faster in searching than a linear linked list. Although the first two nodes are out of balance, the subtree below node 3 is perfectly balanced.

2.7. Integral limits for Gaussian beams

The upper integral limit in Eq. (26) for Gaussian beams is infinity. This problem can be solved using a variable transformation and the integration can be computed by the routine midexp( ) [13]. However, we found that this approach is not computationally efficient. Therefore, we chose to use qtrap( ) instead. We can reduce the upper limit to a finite value by truncating the exponential term in Eq. (26). When

$$|r'' - r| \le KR, \tag{27}$$

or

$$r - KR \le r'' \le r + KR, \tag{28}$$

where K is a constant which can be set in the convolution program CONV, we compute the integrand. Otherwise, we neglect the integrand. For example, if we choose K equal to 4 (which is actually used in the computation for this article) the exponential term in Eq. (26) is about 10^{-14}.

As we discussed in the beginning of this section we compute only the physical quantities in the interval $[0, r_{max}]$, where r_{max} is given by Eq. (22). Combining this limit and Eq. (28), Eq. (26) becomes:

$$C(r, z) = \frac{4P}{R^2}\int_a^b G(r'', z)\exp\left[-2\left(\frac{r''-r}{R}\right)^2\right] I_{0e}\left(\frac{4rr''}{R^2}\right)r''\,dr'', \quad (29)$$

$$a = \mathrm{Max}(0, r - KR), \quad (30)$$

$$b = \mathrm{Min}(r_{max}, r + KR), \quad (31)$$

where the functions Max( ) and Min( ) take the greater and lesser of the two arguments, respectively.

2.8. Integration for circular flat beams

The integrand evaluation for circular flat beams is much simpler than that for Gaussian beams because the integral limits for the flat beams are finite and the evaluation of the integrand causes no overflow. However, the evaluation of $I^{\theta}( )$ in Eq. (18) is also time-consuming. Similar to the integrand evaluation for Gaussian beams, a binary tree is used to store the evaluated $I^{\theta}( )$ to speed up the integration.

Because the integral limits in Eq. (18) for circular flat beams are finite, the integration can be computed directly using the function qtrap( ), and because we compute only the physical quantities in the interval $[0, r_{max}]$, where r_{max} is given by Eq. (22), Eq. (18) rewrites:

$$C(r, z) = P/(\pi R^2)\int_a^b G(r'', z)I_{\theta}(r, r'')2\pi r''\,dr'', \quad (32)$$

where

$$a = \mathrm{Max}(0, r - R), \quad (33)$$

$$b = \mathrm{Min}(r_{max}, r + R). \quad (34)$$

2.9. First interactions inside tissues

In Monte Carlo simulations by MCML [9], the first photon–tissue interactions (unscattered absorption) inside the tissues are scored separately [14]. They are always on the z-axis, and lead to a delta function when the impulse responses of internal probability fluence (cm^{-2}) or absorption probability density (cm^{-3}) are computed. The impulse response can be expressed in two parts:

$$G(r, z) = G_1(0, z)\delta(r)/(2\pi r) + G_2(r, z), \quad (35)$$

where the first term results from the first photon–tissue interactions, and the second from later interactions.

Substituting Eq. (35) into Eq. (29), we obtain:

$$C(r, z) = G_1(0, z)S(r) + \frac{4P}{R^2}\int_a^b G_2(r'', z)\exp\left[-2\left(\frac{r''-r}{R}\right)^2\right] I_{0e}\left(\frac{4rr''}{R^2}\right)r''\,dr'', \quad (36)$$

for Gaussian beams. Substituting Eq. (35) into Eq. (32), we obtain:

$$C(r, z) = G_1(0, z)S(r) + P/(\pi R^2)\int_a^b G_2(r'', z)I_{\theta}(r, r'')2\pi r''\,dr'', \quad (37)$$

for circular flat beams. The comparison between the approaches with and without scoring the first interactions separately will be discussed in the next section.

2.10. Source of error in convolution

In Eqs. (31) and (34) the upper limit of the integration may be limited by r_{max}, which is the grid limit in the r direction during the Monte Carlo simulation. The physical quantities beyond the original grid limit in the r direction do not contribute to the convolution computation, which leads to an error.

For circular flat beams first, from Eq. (34), we know that when

$$r_{max} \geq r + R, \quad (38)$$

Table 1
The optical properties of the three-layered tissue

Layer	n	μ_a (cm^{-1})	μ_s (cm^{-1})	g	Thickness (cm)
1	1.37	1.0	100.0	0.9	0.1
2	1.37	1.0	10.0	0	0.1
3	1.37	2.0	10.0	0.7	0.2

The refractive indices for the top and bottom ambient media are 1.0.

or

$$r \leq r_{max} - R, \tag{39}$$

the limited grid in the r direction does not affect the convolution. Otherwise, the convolution is truncated by the limited grid in the r direction [11]. Therefore, we should not trust the validity of the convolution data for $r \geq r_{max} - R$. In other words, if you want to observe the physical quantity at r in response to a circular flat beam of radius R, the grid limit in the r direction should be large enough so that Eq. (38) holds when you perform the Monte Carlo simulation with MCML.

For Gaussian beams, there are no clean formulas like Eqs. (38) and (39) to describe the valid range because the Gaussian beams theoretically extend to infinity in the r direction. However, the convolution results of a Gaussian beam with a $1/e^2$ radius of R is close to those of a circular flat beam with a radius of R for $r \gg R$ [11]. Therefore, to certain precision we can use the same criteria for circular flat beams (Eqs. (38) and (39)) for Gaussian beams.

3. Sample computation

In this section, we will illustrate the error caused by not scoring the first photon–tissue interactions separately and present a sample convolution run. As an example, the impulse responses were computed by MCML for a tissue described in Table 1. The grid sizes in the r and z directions are both 0.01 cm. The number of grid elements in the r and z directions are 50 and 40, respectively. The number of photon packets traced is 1 000 000. This example took approximately 860 s of computational time on a Silicon Graphics Power Challenge running Irix 6.2.

The impulse response of internal fluence near the tissue surface ($z = 0.005$ cm) is shown in Fig. 2a, where the first interactions were scored separately. If they were scored into the first r grid element it would augment the fluence in the first

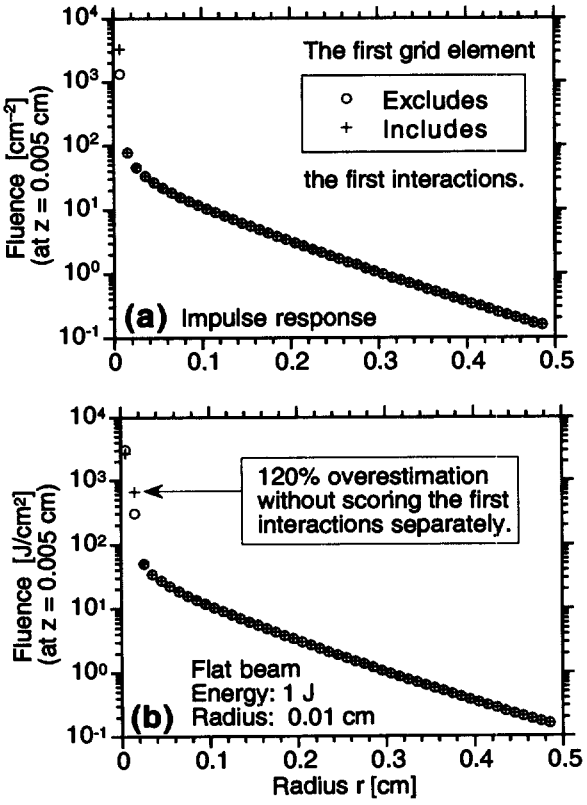

Fig. 2. (a) Impulse response of internal fluence at $z = 0.005$ cm computed by MCML (see Table 1 for tissue configuration). (b) Internal fluence at $z = 0.005$ cm for a circular flat beam. The convolutions with and without scoring the first photon–tissue interactions separately are compared.

grid element by 1.95×10^3 cm^{-2}, compared with the current value of 1.34×10^3 cm^{-2}. We convolved the impulse response over a circular flat beam with an energy of 1 J and a radius of 0.01 cm with and without scoring the first interactions separately for comparison (Fig. 2b). The relative error of the convolved results at $r = 0.015$ cm, which is immediately after the beam radius, is as much as 120%.

We also convolved the impulse response using a Gaussian beam with an energy of 1 J and a radius of 0.1 cm. The convolution error was set to 0.01. The contour lines before and after the convolution are shown in Fig. 3.

4. Conclusions

Based on the Monte Carlo simulation results for impulse responses to an infinitely narrow photon beam normally incident on a multi-layered tissue, one can compute the responses to a collimated photon beam of finite size employing convolution. The convolution avoids time-consuming Monte Carlo simulations for photon beams of finite size and, at the same time, provides the flexibility of computing responses to various beams based on the same impulse response.

The convolution for Gaussian beams and circular flat beams has been coded in ANSI Standard C, therefore, it can run on various computer platforms, e.g. Macintoshes, IBM PC/compatibles, Sun SPARCstations, and IBM RISC/6000 POWERstations. Dynamic data allocation is used in the program, therefore, the number of tissue layers and grid elements can be varied at run time and the computer memory is used efficiently.

The numerical integration in convolution employs an extended trapezoidal rule which allows users to specify the precision. With this approach users need only be concerned about the linearity of the physical quantities to be scored in each grid element when doing Monte Carlo simulations. In contrast if the numerical integration is performed by evaluating the integrand over the original grid elements set up during the Monte Carlo simulation the users must ensure a sufficient number of

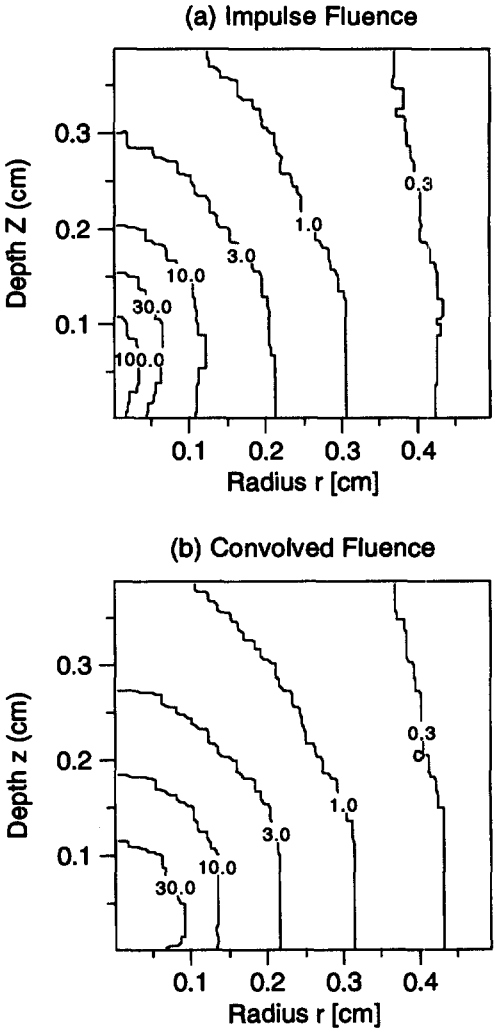

Fig. 3. (a) 2-Dimensional fluence distribution of an impulse response computed by MCML (see Table 1 for tissue configuration). (b) 2-Dimensional fluence distribution of a Gaussian beam of 0.1 cm radius and 1 J energy computed by CONV.

grid elements to be covered by the photon beam of finite size to obtain a reasonable integration precision.

The first photon–tissue interactions inside the tissue should be scored separately which yields a term including a delta function of the radius. The error caused by scoring the first photon–tissue interactions into the first r grid elements instead of separately can be unacceptable in some cases (120% in the example). The error in the low-preci-

sion approaches may be minimized by narrowing the grid size; however, for the Monte Carlo simulations a very small grid size can lead to a large statistical variance in each grid element and a small overall grid system dimension due to computer memory limit.

The CONV and MCML simulation package can be downloaded from the web site at http://biomed.tamu.edu/~lw or through FTP to biomed.tamu.edu (user: conv; password: mcml) or obtained from the authors directly.

Acknowledgements

This work was supported in part by a Whitaker Foundation grant RG94-0060 and National Institutes of Health grants R29-CA68562 and R29-HL45045.

References

[1] B.C. Wilson, G. Adam, A Monte Carlo Model for the absorption and flux distributions of light in tissue, Med. Phys. 10 (1983) 824–830.

[2] S.A. Prahl, M. Keijzer, S.L. Jacques, A.J. Welch, A Monte Carlo model of light propagation in tissue, Proc. SPIE IS 5 (1989) 102–111.

[3] M. Keijzer, S.L. Jacques, S.A. Prahl, A.J. Welch, Light distributions in artery tissue: Monte Carlo simulations for finite-diameter laser beams, Lasers Surg. Med. 9 (1989) 148–154.

[4] S.T. Flock, B.C. Wilson, D.R. Wyman, M.S. Patterson, Monte Carlo modelilng of light propagation in highly scattering tissues—I: model predictions and comparison with diffusion theory, IEEE Trans. Biomed. Eng. 36 (1989) 1162–1168.

[5] S.T. Flock, B.C. Wilson, M.S. Patterson, Monte Carlo modeling of light propagation in highly scattering tissues—II: comparison with measurements in phantoms', IEEE Trans. Biomed. Eng. 36 (1989) 1169–1173.

[6] M. Keijzer, J.W. Pickering, M.J.C. van Gemert, Laser beam diameter for port wine stain treatment, Lasers Surg. Med. 11 (1991) 601–605.

[7] S.L. Jacques, L.-H. Wang, Monte Carlo modeling of light transport in tissues, in: A.J. Welch, M.J.C. van Gemert (Eds.), Optical Thermal Response of Laser Irradiated Tissue, Plenum, New York, 1995, pp. 73–100.

[8] L.-H. Wang, S.L. Jacques, Hybrid model of Monte Carlo simulation diffusion theory for light reflectance by turbid media, J. Opt. Soc. Am. A 10 (1993) 1746–1752.

[9] L.-H. Wang, S.L. Jacques, L.-Q. Zheng, MCML—Monte Carlo modeling of photon transport in multi-layered tissues, Comput. Methods Prog. Biomed. 47 (1995) 131–146.

[10] L.-H. Wang, S.L. Jacques, Optimized radial and angular positions in Monte Carlo modeling, Med. Phys. 21 (1994) 1081–1083.

[11] L.-H. Wang, S.L. Jacques, Monte Carlo Modeling of Light Transport in Multi-layered Tissues in Standard C, University of Texas M.D. Anderson Cancer Center, 1992.

[12] M.R. Spiegel, Mathematical Handbook of Formulas and Tables, McGraw-Hill, 1968.

[13] W.H. Press, B.P. Flannery, S.A. Teukolsky, W.T. Vetterling, Numerical Recipes in C, 2nd ed., Cambridge University Press, Cambridge, 1992.

[14] C.M. Gardner, A.J. Welch, Monte Carlo simulation of light transport in tissue: unscattered absorption events, Appl. Opt. 33 (1994) 2743–2745.